


3-26-2021

Competitive Reductive Removal of Chromate and Perchnetate via Zero-valent Iron

Jonathan Williams Ramirez
Florida International University, jwill363@fiu.edu

Follow this and additional works at: <https://digitalcommons.fiu.edu/etd>

 Part of the [Analytical Chemistry Commons](#), [Environmental Chemistry Commons](#), [Inorganic Chemistry Commons](#), and the [Other Environmental Sciences Commons](#)

Recommended Citation

Williams Ramirez, Jonathan, "Competitive Reductive Removal of Chromate and Perchnetate via Zero-valent Iron" (2021). *FIU Electronic Theses and Dissertations*. 4622.
<https://digitalcommons.fiu.edu/etd/4622>

This work is brought to you for free and open access by the University Graduate School at FIU Digital Commons. It has been accepted for inclusion in FIU Electronic Theses and Dissertations by an authorized administrator of FIU Digital Commons. For more information, please contact dcc@fiu.edu.

FLORIDA INTERNATIONAL UNIVERSITY

Miami, Florida

COMPETITIVE REDUCTIVE REMOVAL OF CHROMATE AND
PERTECHNETATE VIA ZERO-VALENT IRON

A thesis submitted in partial fulfillment of

the requirements of the degree of

MASTER OF SCIENCE

in

BIOMEDICAL ENGINEERING

by

Jonathan Williams Ramirez

2021

To: Dean John Volakis
College of Engineering and Computing

This thesis, written by Jonathan Williams Ramirez, and entitled Competitive Reductive Removal of Chromate and Pertechnetate via Zero-Valent Iron, having been approved in respect to style and intellectual content, is referred to you for judgment.

We have read this thesis and recommend that it be approved.

Yelena Katsenovich

Joshua Hutcheson

Anthony McGoron, Major Professor

Date of Defense: March 26, 2021

The thesis of Jonathan Williams Ramirez is approved.

Dean John Volakis
College of Engineering and Computing

Andrés G. Gil
Vice President for Research and Economic Development
and Dean of the University Graduate School

Florida International University, 2021

ACKNOWLEDGMENTS

I would like to thank my mentors Drs. Yelena Katsenovich, Hilary Emerson, Daria Boglaienko, and Tatiana Levitskaia for giving me the opportunity to develop myself as a researcher. I thank Florida International University's Applied Research Center and Dr. Leonel Lagos for providing me with great facilities and equipment to make my research possible, and Tom Beasley from the Florida Center for Analytical Electron Microscopy for training and use of their instruments. I would also like to thank Dr. Anthony McGoron from the FIU department of Biomedical Engineering for his academic and professional mentorship as a major professor during the acquisition of my Master of Science degree. I also thank my colleagues Antony Arun Maria, and Dr. Shambhu Kandel for their help conducting experiments, and my colleagues Abraham Tadesse Gebru, and Silvina Di Pietro for their support in the laboratory. Finally, I thank the Department of Energy Minority Serving Institution Partnership Program (MSIPP) for their financial support with funding for this project under SRNS contract DE-AC09-08SR22470 and providing me the opportunity to experience two internships in the Pacific Northwest National Laboratory.

ABSTRACT OF THE THESIS
COMPETITIVE REDUCTIVE REMOVAL OF CHROMATE AND
PERTECHNETATE VIA ZERO-VALENT IRON

by

Jonathan Williams Ramirez

Florida International University, 2021

Miami, Florida

Professor Anthony McGoron, Major Professor

Treatment to immobilize radioactive waste is of concern for long-term storage, avoiding future environmental exposure. Most production of Technetium-99 (^{99}Tc) occurred as a byproduct of development of legacy nuclear weapons research. Zero-valent iron (ZVI) is a promising reductant of $^{99}\text{Tc(VII)}$ to a less mobile $^{99}\text{Tc(IV)}$. However, more redox-sensitive contaminants can compete in the reductive process. Therefore, it is important to examine the effects of competitive contaminants and quantify the effects on the reductive removal rates of ^{99}Tc . Chromate, Cr(VI) , is a redox sensitive contaminant that is expected to be present in legacy waste present in the Hanford site's low activity waste streams. The competitive kinetics of Cr(VI) and Tc(VII) reduction by ZVI was studied in basic conditions over a range of Cr(VI) concentrations. The removal rate of $^{99}\text{Tc(VII)}$ slowed down with increasing Cr(VI) concentrations. A second-order kinetic model showed the best fit for the reduction rates of Tc(VII) and Cr(VI) .

TABLE OF CONTENTS

CHAPTER	PAGE
Introduction.....	1
Hypothesis.....	4
Methodology.....	4
Batch Experimental Protocol.....	4
Aqueous Phase Analysis.....	8
Inductively coupled plasma mass spectroscopy (ICP-MS).....	8
Oxidation-Reduction Potential and Dissolved Oxygen.....	9
Solid Phase analysis.....	9
X-ray powered diffraction (XRD).....	9
Scanning electron microscopy (SEM).....	10
Results and Discussion.....	10
Survey of Zero-Valent Iron Materials.....	10
Hepure ZVI Aqueous Analysis via Inductively Coupled Plasma Mass Spectrometry..	14
Measurements of common physicochemical parameters.....	20
Solid Analysis via Scanning Electron Microscope.....	21
Solid Analysis via Energy Dispersive X-ray Spectroscopy (EDS).....	25
Solid Analysis X-Ray Power Diffraction (XRD).....	30
Conclusion.....	32
References.....	35

LIST OF TABLES

TABLE	PAGE
Table 1. Second-order rate constants for Cr(VI) and Tc(VII) reductive removal (1 mg/L ^{99}Tc , 1.2 g/L ZVI, 0.3 M IS NaCl) Note: Rate constants were calculated from measurements up to 8 days for chromium and 24 hours for technetium.	18
Table 2. Oxidation Potential, pH, and Dissolved Oxygen (Aged for 8 Days, 1 mg/L ^{99}Tc , 1.2 g/L ZVI, 0.3 M IS NaCl).....	21
Table 3. EDS Elemental Analysis, Average Mass Percentage (Aged for 8 Days, 1 mg/L ^{99}Tc , 1.2 g/L ZVI, 0.3 M IS NaCl at variable Cr(VI) content)	30
Table 4. XRD estimated percent composition of dried ZVI solids.	32

LIST OF FIGURES

FIGURE	PAGE
<p>Figure 1. Reductive removal via ZVI at 0.3M NaCl in basic conditions (pH = 10.0±0.1) and neutral conditions (7.0±0.1) with 1.2 g/L of ZVI, with constant 50 mg/L Cr(VI) and 1 mg/L Tc(VII) concentrations. Error bars are standard deviation of triplicate samples. (a) Removal of Tc(VII) via different ZVI materials. (b) Removal of Cr(VI) via different ZVI materials.</p>	13
<p>Figure 2. Changes in pH at 0.3M NaCl in basic conditions (pH = 10.0±0.1) and neutral conditions (7.0±0.1) with 1.2 g/L of ZVI, using constant 50 mg/L Cr(VI) and 1 mg/L Tc(VII) concentrations. Error bars are standard deviation of triplicate samples.</p>	14
<p>Figure 3. Reductive removal via Hepure ZVI at 0.3M NaCl in basic conditions (pH = 10.0±0.1). Samples retrieved over 30 days with 1.2 g/L of ZVI, 1 mg/L of Tc(VII) with variable Cr(VI) concentrations. Error bars are standard deviation of triplicate samples. (a) Removal of Tc(VII) in variable Cr(VI) concentrations. (b) Removal of Cr(VI) at variable concentrations.</p>	17
<p>Figure 4. Change in pH over time, 0.3M NaCl in basic conditions (pH = 10.0±0.1). Samples retrieved over 30 days with 1.2 g/L of Hepure ZVI, with variable Cr(VI) concentrations. Error bars are standard deviation of triplicate samples.</p>	19
<p>Figure 5. The visual change in the oxidation of iron in triplicate batches amended with high and low concentrations of chromate. 0.3M NaCl, 1mg/L Tc(VII), in basic pH conditions (pH = 10.0±0.1). Samples aged for 30 days with 1.2 g/L of Hepure ZVI. (Left) Batch containing a “low” initial Cr(VI) concentration of 1mg/L, exhibiting changes in the color of solutions due to iron oxidation and the formation of iron oxides that were further identified by XRD analyses. (Right) Batch containing a high initial Cr(VI) concentration of 50mg/L, with little change to solution color evident of little iron oxidation.</p>	20
<p>Figure 6. Scanning Electron Microscope (SEM) 8 Day Aged Samples, x10,000 magnified, 20.0 kV. 0.3M NaCl, 1mg/L Tc(VII), 1 mg/L Cr(VI) in basic pH conditions (pH = 10.0±0.1) with 1.2 g/L of Hepure ZVI. Observed formations will be used to later assess the morphology of the oxidized iron surface. (a) spherical formation, (b) acicular formation, (c) porous formation with surface oxidation, (d) spherical and hexagonal formations.</p>	23
<p>Figure 7. Scanning Electron Microscope (SEM) 8 Day Aged Samples, x10,000 magnified, 20.0 kV. 0.3M NaCl, 1mg/L Tc(VII), 10 mg/L Cr(VI) in basic pH conditions (pH = 10.0±0.1) with 1.2 g/L of Hepure ZVI. Observed formations will be used to later assess morphology of iron (a) acicular formation, (b) little oxidation with two spherical formations, (c) flake-like formation. (d) spherical formation.</p>	24

Figure 8. Scanning Electron Microscope (SEM) 8 Day Aged Samples, x10,000 magnified, 20.0 kV. 0.3M NaCl, 10 mg/L Cr(VI) in basic pH conditions (pH = 10.0±0.1) with 1.2 g/L of Hepure ZVI. Zoomed in is formation of hexagonal iron oxide morphology indicating presence of magnetite [15]. 24

Figure 9. Behavior of iron solids inside batch solutions after 30 days. (a) 1 mg/L Cr(VI) shows brown coloration and some magnetic species. (b) 50 mg/L Cr(VI), shows greater amount of magnetic species, with little coloration led by iron oxidation. . 25

Figure 10. Most representative spectrum from Scanning Electron Microscope (SEM) 8-day aged samples, x250 magnified, 20.0 kV. 0.3M NaCl, 1mg/L Tc(VII), in basic pH conditions (pH =10.0±0.1) with 1.2 g/L of Hepure ZVI. (a) 1 mg/L Cr(VI), (b) 10 mg/L Cr(VI). (Left) Shows SEM image with highlighted area of where most representative spectra was collected. (Top right) Shows the collected spectra of SEM, and the elemental matches collected. (Bottom Right) Shows the resulting elemental composition calculated. Note Technetium is highlighted red due to its concentration being below the limits of detection. 27

Figure 11. EDS map images from 8 day aged samples, x250 magnified, 20.0 kV. 1 mg/L of Cr(VI) 0.3M NaCl, 1mg/L Tc(VII), in basic pH conditions (pH = 10.0±0.1) with 1.2 g/L of Hepure ZVI. Brighter areas signify higher weight percentage of each element. 28

Figure 12. EDS map images from 8 day aged samples, x250 magnified, 20.0 kV. 10 mg/L Cr(VI) 0.3M NaCl, 1mg/L Tc(VII), in basic pH conditions (pH = 10.0±0.1) with 1.2 g/L of Hepure ZVI. Brighter areas signify higher weight percentage of each element. 29

Figure 13. XRD pattern comparison of pristine ZVI (first pattern), and of each of the dried solids from the batch experiments (second to sixth pattern), versus peaks from the Crystallography Open Database XRD database (seventh to eleventh pattern) and International Centre for Diffraction Data's PDF database.31

Introduction

Long-term treatment of nuclear-bearing waste is a concern for many industries. Radioactive waste can come from several sources, like energy and fuel production, medical procedures, and weapons manufacturing. For example, ^{99m}Tc is widely used in medicine as a radioactive tracer. ^{99m}Tc quickly degrades to ^{99}Tc within hours, which then must be disposed of [2].

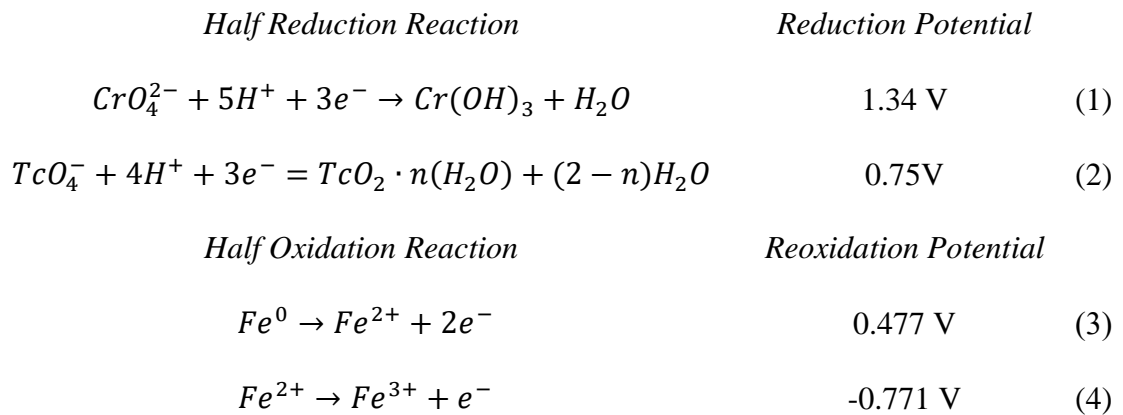
Treatment of complex waste, composed of different chemicals, can be especially challenging and thus is a substantial goal for the United States' Department of Energy (DOE). The Hanford Site in Washington State is one of the largest repositories of legacy nuclear waste in the world [2]. Due to its complex nature, the DOE has a long-term treatment plan for the immobilization of radioactive waste in glass form for long-term storage and disposition [3].

Technetium-99 (^{99}Tc) is of primary concern for permanent disposal of low activity waste (LAW) by vitrification due to its high volatility, leading to only partial incorporation into a glass waste form. ^{99}Tc 's long half-life of 213,000 years makes long term immobilization preferable for treatment [4]. At a high melting temperature of 1150 °C, ^{99}Tc is volatilized and captured by an off-gas condensate waste stream, which is then recycled back to a LAW glass melter feed. The presence of the low-level beta emitter ^{99}Tc in the form of pertechnetate $^{99}\text{Tc}(\text{VII})$ in the off-gas condensate is of great concern for the efficiency of vitrification. The off-gas recycle disproportionately increases loading of ^{99}Tc and other problematic contaminants, such as chromate, impeding overall LAW processing and complicating the treatment process [3,5]. Pegg et al. estimated that only 35% of technetium

was retained as the glass waste in a single pass through the vitrification process [6]. $^{99}\text{Tc(VII)}$ as pertechnetate (TcO_4^-) is highly soluble and mobile, increasing the difficulty of long term storage of waste.

Alternative treatment methods for ^{99}Tc to circumvent the recycle of an off-gas condensate would be helpful, avoiding recycle of the waste stream with vitrification. Reductive separation, the process where a reductant is used to immobilize contaminants, has been used as a treatment option in many similar applications. Technetium that is in substantially reducing conditions will be in the form of Tc(VI) which is far less mobile than Tc(VII) due to its very low solubility [7]. Zero-valent iron (ZVI) has been used for treatment for remediation in many different applications [8]. Using a cost-efficient, readily available reductant like ZVI is of interest for large scale industrial applications. On the surface of the iron particle, an oxide layer forms reducing possible contaminants like ^{99}Tc . Different manufacturing methods of ZVI powder can affect its capabilities to be used for reductive separation. Previous experiments by Boglaienko et al. on different ZVI materials efficiency for the reductive removal of Tc(VII) showed that ZVI manufactured by the electrolytic method posed the greatest capabilities for treatment [9]. Particle size also had a significant effect on reductive capability, as smaller particle sizes can provide more surface area increasing speed of reduction, although smaller mesh sizes led to more agglomeration of particles which negated their benefits [9]. The redox chemistry of ^{99}Tc supports ZVI as a viable reductant [10]. If reduced, the $^{99}\text{Tc(VII)}$ could be changed to its less mobile form $^{99}\text{Tc(IV)}$ as an alternative treatment method for the off-gas condensate [4]. $^{99}\text{Tc(IV)}$ provides low solubility and mobility, easing long term immobilization.

When using ZVI for reductive separation of $^{99}\text{Tc(VII)}$, other co-contaminants must be considered as they can affect treatment efficiency. The off-gas condensate contains 50-135 times more Cr(VI) in the form of chromate than $^{99}\text{Tc(VII)}$ [3]. Chromium has anti-corrosive properties, which can passivate the surface of the iron material, slowing down the reductive separation process. Tc(VII) as pertechnetate ion has also been shown to have anti-corrosive properties, which could further inhibit iron oxidation [11,12]. Cr(VI) may compete with ^{99}Tc reduction as it can be reduced to Cr(III) more favorably compared to $^{99}\text{Tc(VII)}$ reduction to $^{99}\text{Tc(IV)}$. This can be seen by comparing the redox chemistry of both reactions [10,13]. NaCl was used in the solution, increasing ionic strength, as a complex combination of different salts expected in the off-gas.



The goal of this research is to assess the efficiency of ZVI as a treatment method for ^{99}Tc reduction with variable concentrations of a competing contaminant like Cr(VI).

Objective

The objective of the experimental work is twofold: 1) investigate changes in the kinetics of the reductive removal of technetium through the application of zero-valent iron in the presence of competitive contaminants, specifically chromate; 2) determine the effect of a

co-located competitor, like chromate, on the reductive separation of pertechnetate by zero-valent iron.

Hypothesis

Low activity waste's off-gas condensate contains an estimated 50-135 times more Cr(VI) than $^{99}\text{Tc(VII)}$. This study hypothesizes that Cr(VI) in the form of chromate will significantly affect the reduction of pertechnetate $^{99}\text{Tc(VII)}$ by ZVI by slowing down the reduction kinetics of $^{99}\text{Tc(VII)}$. Cr(VI) reduction has a higher redox potential compared to $^{99}\text{Tc(VII)}$, hence chromate is expected to be reduced more readily compared to technetium. Chromium and technetium are both known inhibitors of iron corrosion slowing the oxidation of the zero-valent iron, further slowing down Cr(VI) and $^{99}\text{Tc(VII)}$ reduction kinetics [11].

Methodology

Batch Experimental Protocol

Batch experiments were performed to measure the effect of variable Cr(VI) concentrations on the reductive removal kinetics of $^{99}\text{Tc(VII)}$ and Cr(VI) by ZVI in aerobic conditions. Studying the reductive process in aerobic conditions allows for more translatable results by resembling real-field treatment conditions. Samples were prepared in triplicate with a variable chromate concentration ranging from 1 mg/L to 50 mg/L. All samples were prepared in a 0.3 M sodium chloride (NaCl) matrix at basic pH conditions (10 ± 0.1) and amended with a constant concentration of 1mg/L of $^{99}\text{Tc(VII)}$. NaCl was used to provide the ionic strength of the solution which is expected in the off-gas waste stream. Experiments were performed in basic conditions to slow down the reductive process,

allowing for more accurate estimates of the kinetic rates of reduction. The initial solutions were prepared volumetrically before being contacted to ZVI powder. Deionized water (DIW) was collected from Barnstead NANOpure® Diamond System with a $>18\text{m}\Omega$ -cm resistance, indicating minimal foreign ion levels and eliminating any possible variability caused by impurities.

Comparisons were done on different manufactured ZVI to compare their effectiveness for reductive separation. Three materials were compared in basic pH conditions of 10.0 ± 0.1 with 50 mg/L of Cr(VI), Hepure ZVI (Ferox PRB reactive iron powder, 95% iron, 297 μm (50 mesh), Hepure Technologies Inc, cast iron powder), Fisher Scientific electrolytic ZVI (Hampton, NH, 75 μm (200 mesh), Fisher Scientific, iron powder), ZVI granules (Alfa Aesar, Electrolytic Iron granules, 1-2 mm). Boglajenko et al., (2019) performed a survey of ZVI materials and found that out of the iron materials tested, Fisher 200 mesh electrolytic ZVI had the most promising performance [9]. Hepure and Fisher iron powder were also compared under neutral pH conditions, 7.0 ± 0.1 . Hepure ZVI showed the most promising results for contaminant removal and was used for subsequent batches comparing the effect of competitive contaminants on the reductive removal process.

For each batch, 175 mL of the solution was prepared volumetrically for each Cr(VI) concentration tested, where 40 mL was used for each of the triplicates and a no-ZVI control sample. Sodium chloride (NaCl, ACS reagent grade, Fisher Chemical) was used to simulate salt levels that have been predicted to be in the off-gas condensate. To make a 0.3 M NaCl 175 mL batch solution, 3.068 g of NaCl salt was weighted. Chromium standard (1000 $\mu\text{g/L}$ Cr^{+6} , $\text{K}_2\text{Cr}_2\text{O}_7$, Purity 99.998% in H_2O , High Purity Standard) was added in the batch solution, at variable concentrations per batch (1, 5, 25, 10, 50 mg/L) alongside the salt and

diluted up to 175 mL with ultrapure water. Technetium-99 stock solution was procured from Eckert and Ziegler (3 mCi, Valencia, CA) and diluted to make a stock solution for all experiments. 0.379 mL of stock solution was diluted in 20 mL of ultrapure DI water. The solution was made with a target concentration of ^{99}Tc of 4.5 mM. The ^{99}Tc concentration of the stock solution was independently checked using both inductively coupled plasma-mass spectrometer (ICP-MS, ThermoFisher Scientific iCAP RQ) and a liquid scintillation counter (LSC, Tricarb 2910 TR, Perkin Elmer) to assure accuracy. LSC was used to measure the beta activity of 50 μL of the prepped ^{99}Tc solution with 10 mL of Ultima Gold liquid scintillation cocktail, measured for 10 minutes. The average measured concentration was calculated based on triplicate measurements, and the measured concentration of the stock to be 4.217 mM. This solution was used to prepare a set of eight calibration standards diluted in 2% HNO_3 for ICP-MS ranging from 0.005-1000 $\mu\text{g/L}$, with a measured calibration R^2 of 1.00.

From the ^{99}Tc stock, 405 μL was pipetted to the 175 mL batch solution to reach a 1.0 mg/L concentration in all samples. The solution was then amended with 100 μL of 1.0M NaOH to approach basic pH conditions and avoid dilution caused by adjusting of pH. Subsequently, the pH was adjusted using 0.1 M sodium hydroxide and hydrochloric acid solutions to a pH of 10 ± 0.1 . The pH was measured using a meter (Orion Star A215 with Orion 8156BNUWP Ross Ultra electrode) and calibrated using three different buffer solutions encompassing a wide pH range (4.01, 7.00, 10.01) assuring a linear fit $>95\%$. No pH adjustments were done after the solution contacted the ZVI.

Next, the dry reductant was weighed, 48 ± 1 mg of Hepure ZVI for a 1.2 g/L concentration in 40 mL vials. The pH-adjusted solutions amended with 1 mg/L of $^{99}\text{Tc(VII)}$, and variable

Cr(VI) were distributed between ZVI-amended triplicate samples and no-ZVI control prepared to test for the initial Cr and ^{99}Tc concentrations. Samples were capped and placed on an end-over-end rotator (Thermo Fischer Scientific, Waltham, MA) at 25 rpm throughout the experiment (30 days) except during sampling for later liquid phase analysis. Sampling was done in different time intervals (10 minutes, 1 hour, 3 hours, 1 day, 2 days, 5 days, 8 days, and 30 days) to measure the kinetics of reductive removal of both technetium and chromium. A negligible volume of sample ($<500\ \mu\text{L}$) was removed during each sampling event, so the total volume removed was not higher than 10% at the end of the sampling period to minimize any effect on the solid to liquid ratio. Removed samples were filtered via a $0.2\ \mu\text{m}$ pore size syringe filter (PTFE, Fisher Scientific). The filtered liquid was pipetted on to a test tube containing 2% nitric acid solution and analyzed via inductively coupled plasma mass spectroscopy, (ICP-MS) for ^{99}Tc and Cr. The removal reduction rate was determined using a second-order kinetics model.

Extra batch samples were prepared by following the same methodology to conduct solid characterization studies. After 8 days of contact with ZVI, samples were centrifuged at 4500 rpm for 15 minutes. The supernatant was removed using a transfer pipette and the solids were then rinsed using deoxygenated nitrogen purged ultrapure de-ionized water (DIW) to remove salts. To deoxygenate the DIW, nitrogen gas was bubbled into the DIW at a steady rate for 15 minutes to remove any oxygen in the DIW that could alter the iron oxide phases through oxidation. After the purged water was added, the same process was repeated to remove the liquids and isolate the solids. Rinsed ZVI samples were placed in a vacuum oven (Thermo Fischer Scientific, Waltham, MA) at 25 in Hg and a temperature of

35°C for drying and then used for solids characterization via X-ray diffraction and microscopy analysis.

Aqueous Phase Analysis

Inductively coupled plasma mass spectroscopy (ICP-MS)

For ⁹⁹Tc and Cr analyses, liquid aliquots were diluted in 2% nitric acid (HNO₃) and analyzed via ICP-MS (Thermo Fisher Scientific, iCAP RQ) in the kinetic energy discrimination (KED) mode. The calibration of the instrument was accomplished with 3-4 replicate measurements, a dwell time of 0.1 seconds, a wash time of 30 seconds, and a delay time of a minimum of 30 seconds. Limits of quantification (LOQ) of the elements were calculated as 0.003 μg/L for ⁹⁹Tc and 0.024 μg/L for Cr. Reduction kinetics of the removal of both Cr(VI) and ⁹⁹Tc(VII) was calculated using both concentrations in the liquid phase over time using the experimental data.

Different kinetic models were used to fit the data obtained to describe the reductive removal of both contaminants. A rate constant was obtained for each batch from the kinetic models which describe the speed of the removal of both contaminants. The data was fit to a first and second-order kinetic model, described by the following equations.

$$\ln[C_t] = k_{1\text{st Order}} t + \ln[C_0] \quad (5)$$

$$\frac{1}{[C]_t} = k_{2\text{nd Order}} t + \frac{1}{[C]_0} \quad (6)$$

Where t is the time in minutes, $[C]$ is the concentration of ⁹⁹Tc(VII) or Cr(VI) over time, and k is the rate constant.

Oxidation-Reduction Potential and Dissolved Oxygen

The oxidation-reduction potential (ORP) and dissolved oxygen (DO) were measured for batches used for solid-phase analysis at the end of their 8-day aging time. ORP was measured using an Orion Star A215 meter with a Mettler Toledo EM40-BNC 30043106 Fisher brand Accumet electrode and DO with an Orion Star A123 meter and a Thermo Scientific polarographic probe 083005MD. Before measurements were taken, both electrodes were calibrated. The performance of the ORP electrode was verified using the standard hydrogen electrode (SHE) standard solution (Orion, Thermo Fischer Scientific, Waltham, MA), while the DO electrode was calibrated by taking into account the oxygen measured in the air.

Solid Phase analysis

X-ray powered diffraction (XRD)

Sacrificial samples were prepared for solid-phase analysis and were aged for eight days, when $^{99}\text{Tc(VII)}$ concentration was the lowest. After 48 hours, solid samples were placed in an anaerobic glove box to prevent further iron oxidation. Dried solids for XRD were scraped and placed in a mortar to achieve finer solid grain to minimize the noise in the XRD signal, minimal grounding was performed to keep integrity in the crystal formation in the solid. The solid sample was then packed and flattened in a sample holder for analysis. The packed sample was run via Bruker D2 PHASER X-ray diffractometer equipped with a built in chiller, LYNXEYEEXET (1D mode, opening $5^\circ 2\theta$ detector, analyzing from a 2θ value of $10\text{-}90^\circ$ with a 0.02° step size. The analysis lasted for one hour, and afterwards, the sample was removed from the sample holder and placed back in anaerobic conditions. The resulting patterns were compared to the crystallography open database (COD), and the

International Centre for Diffraction Data's power diffraction file database (PDF) to semi-quantitatively estimate the relative concentration of different iron oxides species within the solid phase, as well as the elemental composition of the solid samples [14]. The obtained patterns were matched using the DIFFRAC.EVA V5.1 XRD software.

Scanning electron microscopy (SEM)

Part of the dry solid ZVI sample was placed on conductive carbon tape atop of an aluminum metal specimen stub. Surface characterization was conducted via a JEOL IT500HR Field Emission Microscope (SEM) equipped with the Bruker XFlash 6160 energy-dispersive x-ray spectroscopy (EDS) with a 60 mm window SDD detector. Energy dispersive spectroscopy (EDS) was performed to find the elemental composition of the solids, allowing for comparisons with acquired XRD data. Identification of elements and their quantification during spectra acquisition was done via the Bruker Esprit software. EDS power was set to a voltage of 15 keV, and images were obtained at different magnifications of 250x-10,000x. Elemental composition was based on the average measurement on different spectra, gathered on 10 separate points on each sample surface.

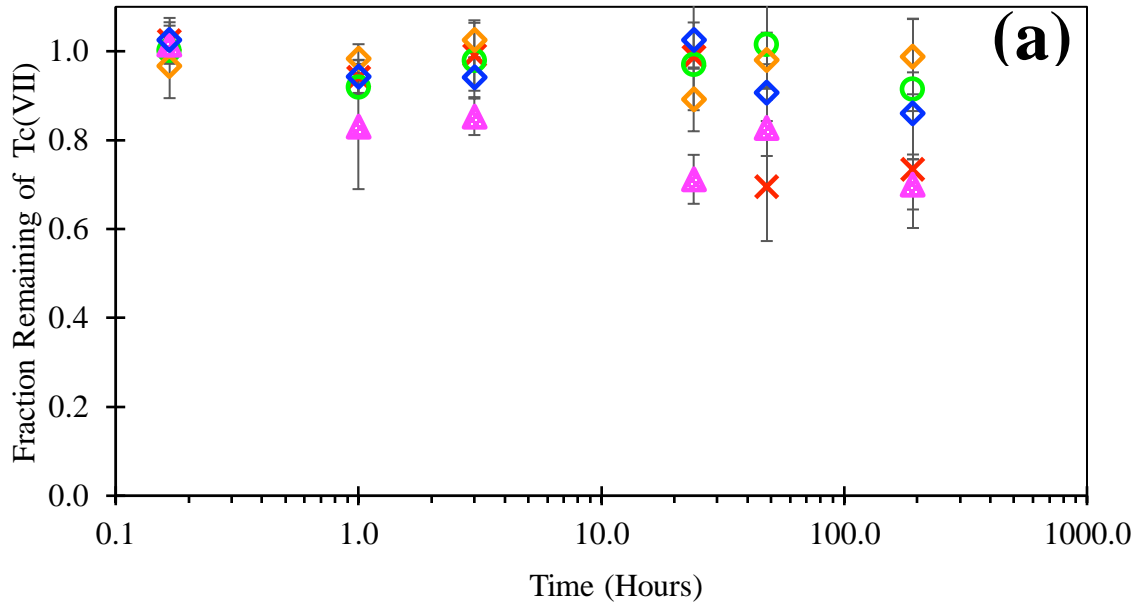
Results and Discussion

Survey of Zero-Valent Iron Materials

Comparison of removal between electrolytically manufactured ZVI, ZVI granules, and cast iron ZVI showed different removal efficiencies. Experiments were done in basic pH conditions; between all materials, Hepure cast iron ZVI and Fisher Scientific electrolytic 200 mesh ZVI had the best performance in contaminant removal. Subsequent tests were done to compare reduction between Hepure ZVI and Fisher 200 mesh ZVI in both basic

and neutral pH conditions ($\text{pH} = 7.0 \pm 0.1$ and 10.0 ± 0.1); the removal of both contaminants was favored in neutral pH conditions. Hepure ZVI showed the best removal of contaminants compared to all other electrolytic ZVI materials. Figure 1 summarizes the efficiency of ZVI materials for experiments comparing the removal of both contaminants, (a) for Tc(VII) and (b) for Cr(VI). Hepure ZVI in basic conditions was more efficient compared to 200 mesh ZVI in neutral pH conditions, both Tc(VII) and Cr(VI) fractions were lower for basic pH Hepure compared to neutral pH Fisher 200-mesh ZVI. A t-test was performed on the remaining fraction of chromium after 8 days comparing basic Hepure ZVI and neutral 200-mesh Fisher ZVI and showed a significant difference favoring removal by Hepure even in basic conditions ($P=6.8\text{e-}04 < 0.05$). Figure 2 shows pH over time with different ZVI materials in the same conditions. The initial spike in pH in batches with neutral initial pH conditions is likely due to OH^- ions released during iron oxidation.

Remaining Fraction of Tc(VII)
ZVI Material Comparison



× Basic pH, Hepure ZVI

○ Basic pH, ZVI Granules

◇ Basic pH, 200 Mesh ZVI

△ Neutral pH, Hepure ZVI

◇ Neutral pH, 200 Mesh ZVI

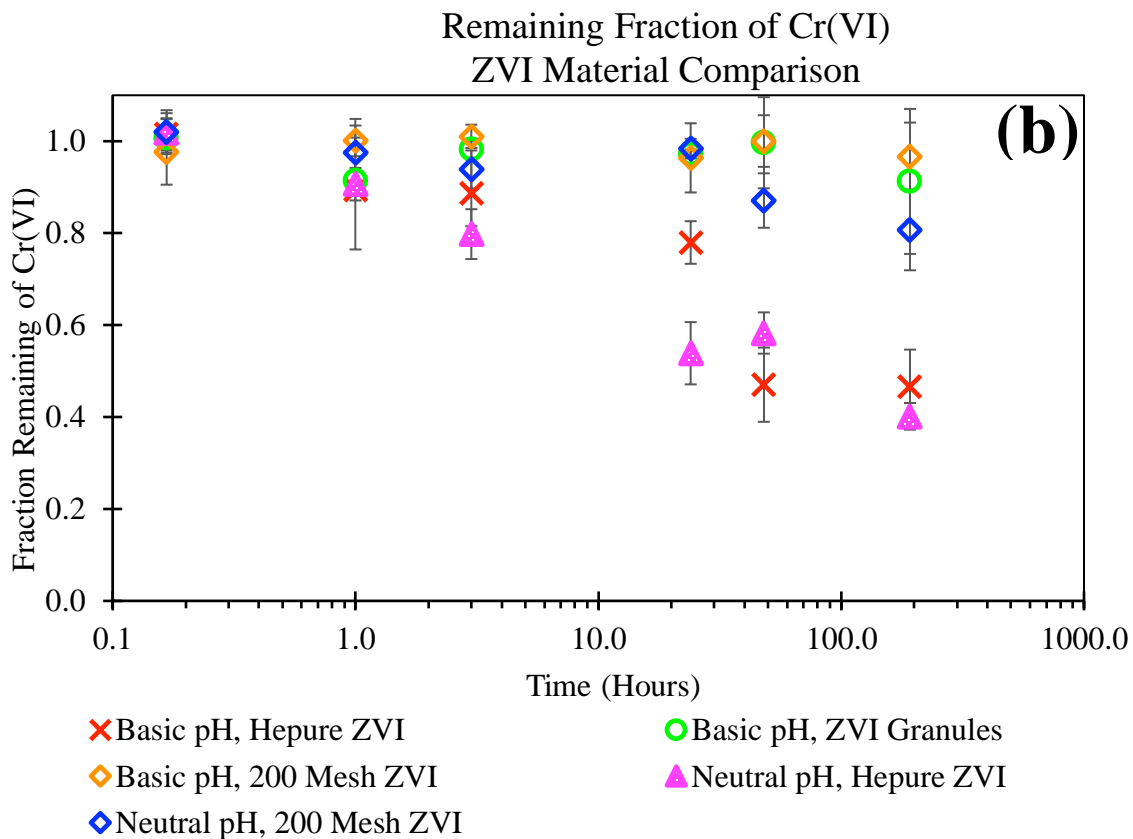


Figure 1. Reductive removal via ZVI at 0.3M NaCl in basic conditions ($pH_i = 10.0 \pm 0.1$) and neutral conditions (7.0 ± 0.1) with 1.2 g/L of ZVI, with constant 50 mg/L Cr(VI) and 1 mg/L Tc(VII) concentrations. Error bars are standard deviation of triplicate samples. **(a)** Removal of Tc(VII) via different ZVI materials. **(b)** Removal of Cr(VI) via different ZVI materials.

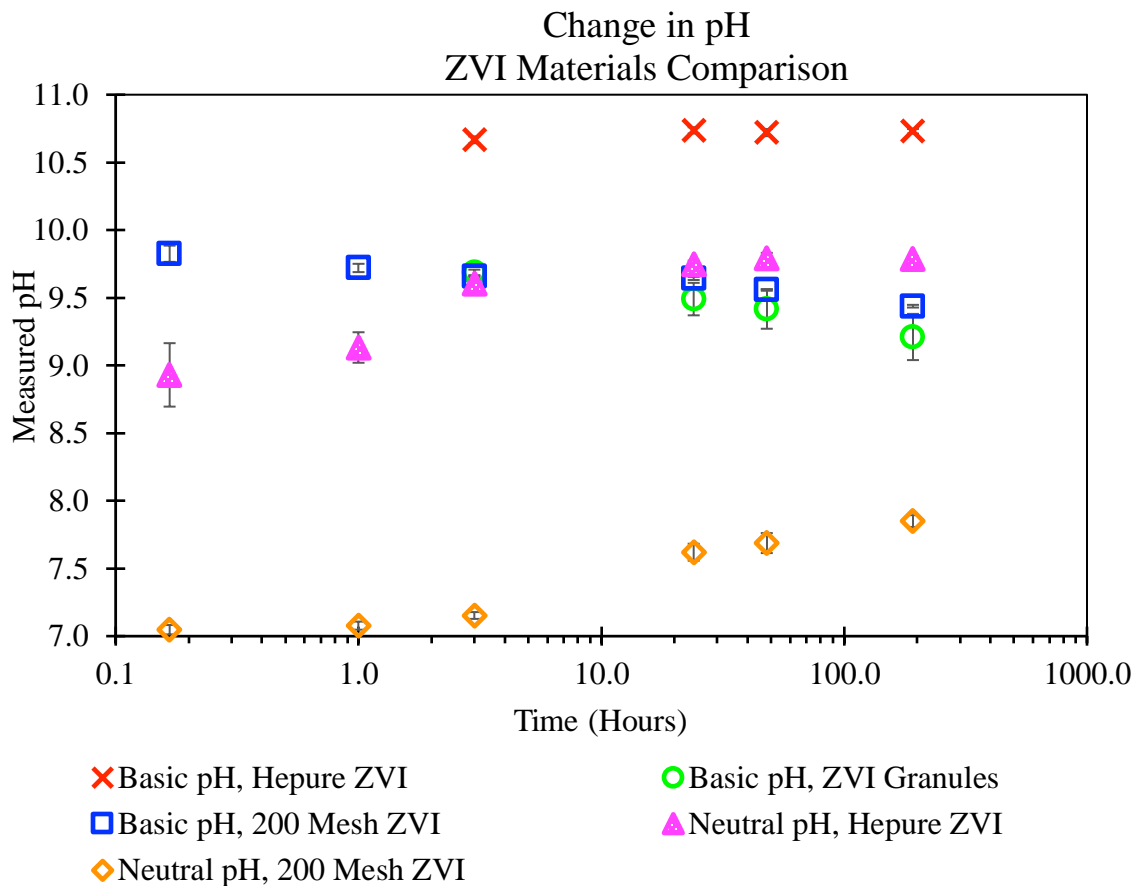


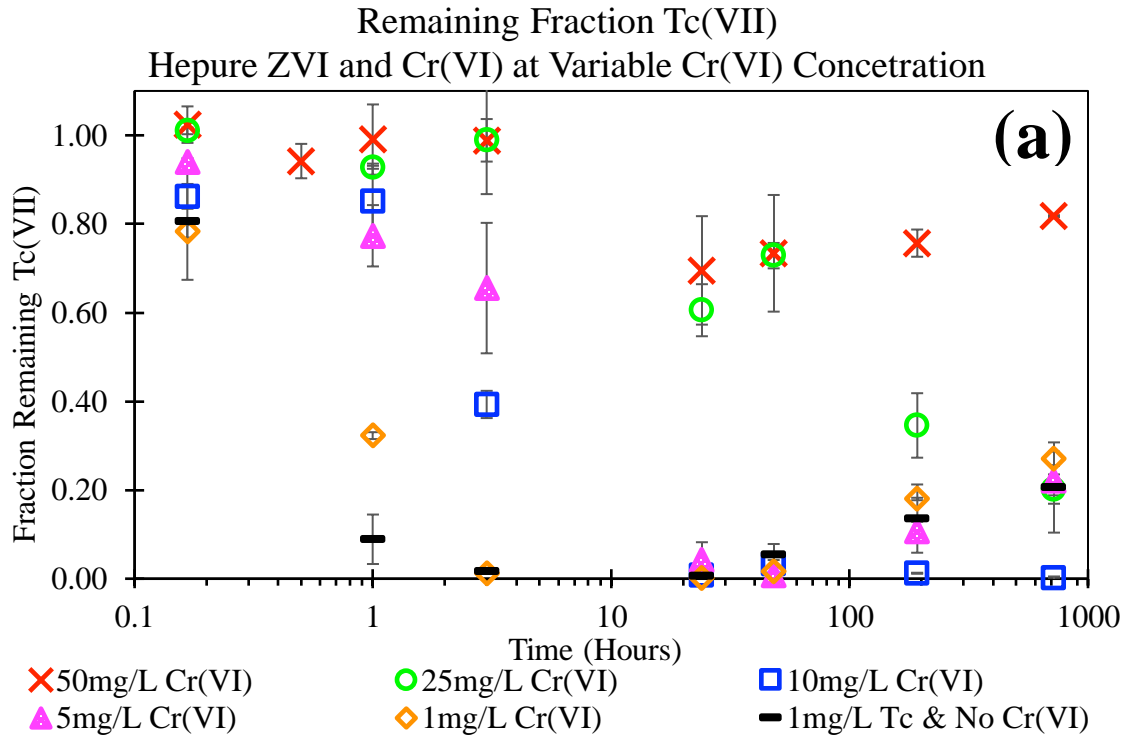
Figure 2. Changes in pH at 0.3M NaCl in basic conditions ($pH_i = 10.0 \pm 0.1$) and neutral conditions (7.0 ± 0.1) with 1.2 g/L of ZVI, using constant 50 mg/L Cr(VI) and 1 mg/L Tc(VII) concentrations. Error bars are standard deviation of triplicate samples.

Hepure ZVI Aqueous Analysis via Inductively Coupled Plasma Mass Spectrometry

A second-order kinetic model showed a good fit for the reductive kinetics of Cr(VI) and $^{99}\text{Tc(VII)}$ seen in Table 1. As expected, the reductive removal process was impacted by the concentration of competitive contaminants like chromate in the solution as seen in Figure 3, depicting the remaining aqueous fraction of each contaminant over time via reductive separation in different chromium concentrations in basic pH conditions (10 ± 0.1) and 0.3 M NaCl. Higher concentrations of chromium exhibited a trend toward lower rates of reductive removal for both chromium and technetium. The highest rates of reduction were

seen at the initial sampling points of the experiments, indicating faster initial reductive removal. Later time points have a lower change in contaminant concentration, as the solutions reach equilibrium conditions. The initial speed of reductive removal is consistent with the assessment that the pristine iron will initially take a greater part in reductive removal but will slow down due to the oxide layer formation at the outside of the iron particle, passivating the particle core for further oxidation. This effect is further amplified by the passivation/anti-corrosive properties of chromium and technetium.

The concentration of Tc(VII) in the form of pertechnetate anion is of the highest concern. Variation of initial chromium concentration played a large role in the removal of technetium. At the highest chromium concentration tested, the aqueous fraction of Tc(VII) did not decrease past 0.70, supporting that technetium is predominantly removed after most chromate is removed. This is supported by the reduction potential of pertechnetate and chromate anions. Measured Tc(VII) concentration was predominantly the lowest, 24 hours after contact with the ZVI powder. Batches with an initial concentration of 25 mg/L or less of chromate exhibited removal of almost all technetium (>95% removal) at their lowest fraction remaining value. At the end of the sampling points, reoxidation of technetium, likely caused by atmospheric oxygen diffused to the solution, led to an increase in the measured aqueous fraction of Tc(VII). At the final sampling point, there was reoxidation of Tc up to 30%, yet reoxidation rates were not consistent overall due to variations in the exposure to oxygen. Second-order kinetics proved to be a good model, with better R^2 in all batches compared to a first-order kinetics model, to describe the reductive removal of both chromium and technetium with Hepure ZVI, shown in Table 1. A first-order kinetic model was also used to model removal but was less effective in describing the removal behavior.



Remaining Fraction Cr(VI)
Hepure ZVI and Tc(VII) at Variable Cr(VI) Concentration

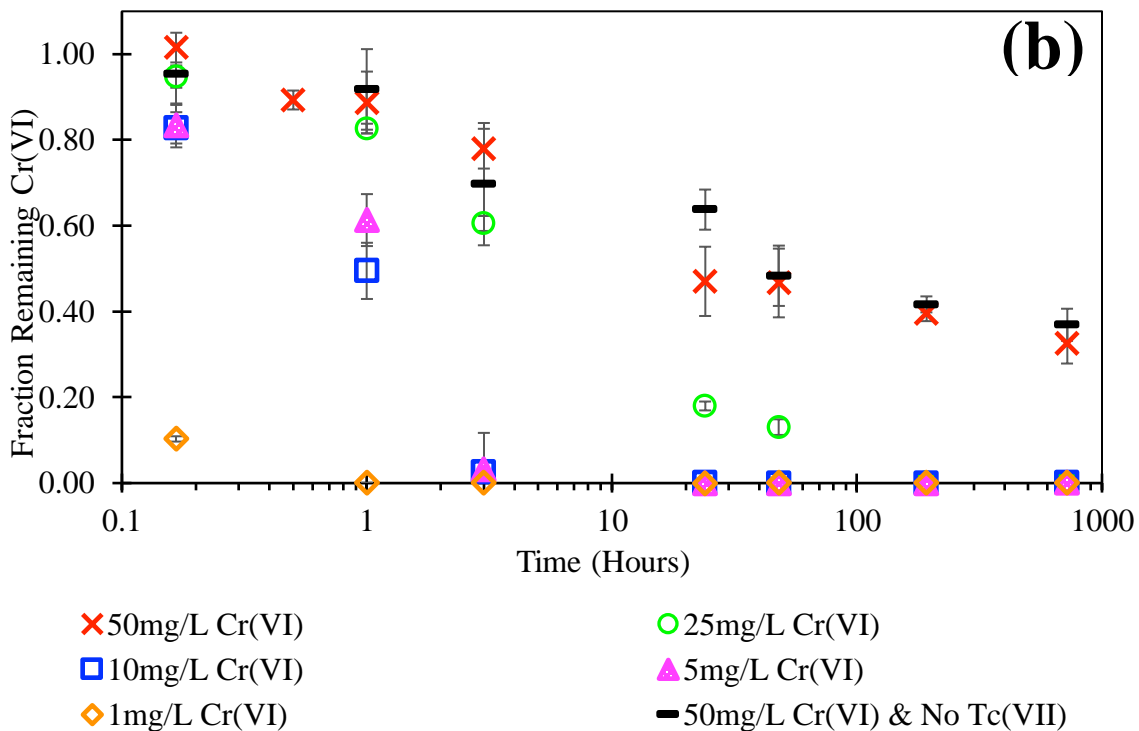


Figure 3. Reductive removal via Hepure ZVI at 0.3M NaCl in basic conditions ($pH_i = 10.0 \pm 0.1$). Samples retrieved over 30 days with 1.2 g/L of ZVI, 1 mg/L of Tc(VII) with variable Cr(VI) concentrations. Error bars are standard deviation of triplicate samples. **(a)** Removal of Tc(VII) in variable Cr(VI) concentrations. **(b)** Removal of Cr(VI) at variable concentrations.

Table 1. Second-order rate constants for Cr(VI) and Tc(VII) reductive removal (1 mg/L ⁹⁹Tc, 1.2 g/L ZVI, 0.3 M IS NaCl) Note: Rate constants were calculated from measurements up to 8 days for chromium and 24 hours for technetium.

Initial Cr(VI) (mg/L)	Cr k_{Cr} ($M^{-1}hr^{-1}$)	95% Confidence Interval [CI_{Cr}]	R^2
50	9.74×10^{-10}	4.33×10^{-10} to 1.51×10^{-9}	0.862
25	3.29×10^{-06}	2.16×10^{-06} to 4.42×10^{-06}	0.942
10	2.01×10^{-04}	8.70×10^{-05} to 3.15×10^{-04}	0.857
5	2.03×10^{-03}	1.74×10^{-03} to 2.32×10^{-03}	0.994
1	2.24×10^{-03}	-1.55×10^{-03} to 6.03×10^{-03}	0.764
50 (No Tc)	2.16×10^{-9}	4.23×10^{-10} to 3.90×10^{-09}	0.749
0	-----	-----	-----

Initial Cr(VI) (mg/L)	Tc-99 k_{Tc} ($M^{-1}hr^{-1}$)	95% Confidence Interval [CI_{Tc}]	R^2
50	3.27×10^{-08}	2.72×10^{-08} to 3.82×10^{-08}	0.992
25	5.12×10^{-07}	-2.97×10^{-07} to 1.32×10^{-06}	0.788
10	7.43×10^{-06}	1.51×10^{-06} to 1.33×10^{-05}	0.996
5	1.79×10^{-05}	1.31×10^{-05} to 2.28×10^{-05}	0.992
1	7.58×10^{-04}	6.48×10^{-04} to 8.68×10^{-04}	0.998
50 (No Tc)	-----	-----	-----
0	9.36×10^{-05}	1.16×10^{-05} to 1.75×10^{-04}	0.923

Experimental batches also qualitatively displayed visual signs of iron passivation by Cr(VI). Figure 5 shows a comparison between the batches with the highest and lowest concentration of Cr(VI), 1 mg/L, and 50 mg/L. The low concentration batch shows a murky and brown solution, compared to the high concentration batch which remained clear with yellow color from the Cr(VI). The difference in color between the two batches implies a

greater formation of iron oxides with Fe(II) and Fe(III) in batches containing low levels of Cr(VI). This supports that the change in the speed of the reductive removal kinetics in different Cr(VI) concentrations is led by a change in iron oxidation caused by the chromium inhibition effect on the formation of iron oxides.

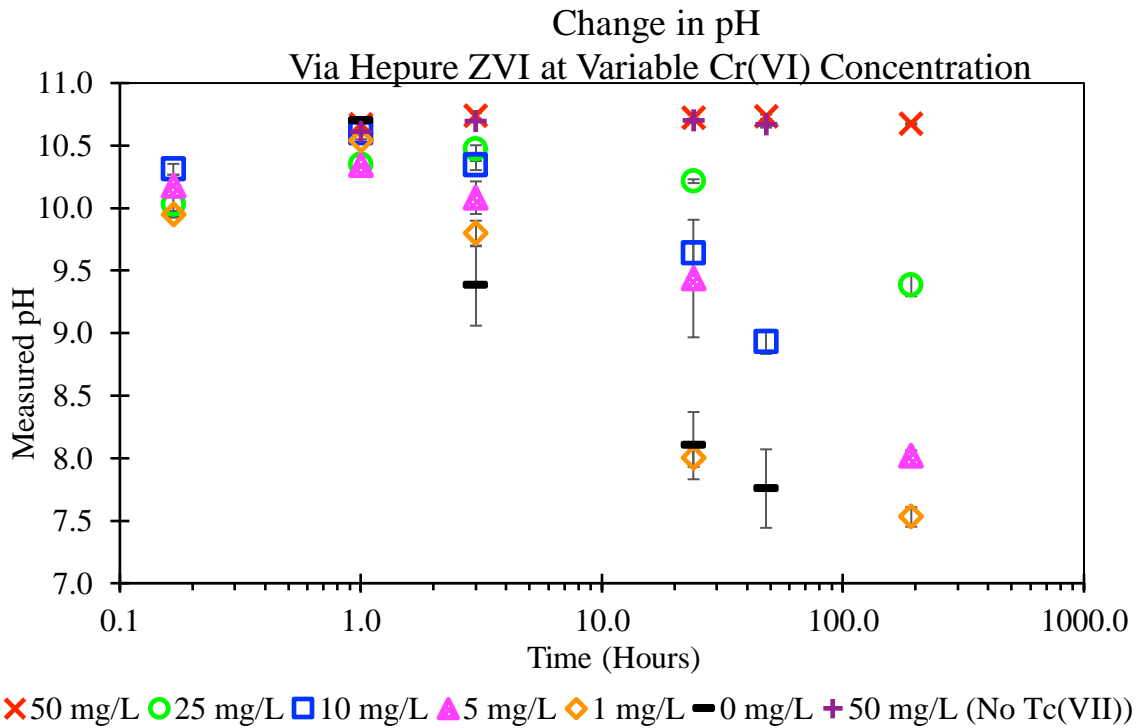


Figure 4. Change in pH over time, 0.3M NaCl in basic conditions ($pH_i = 10.0 \pm 0.1$). Samples retrieved over 30 days with 1.2 g/L of Hepure ZVI, with variable Cr(VI) concentrations. Error bars are standard deviation of triplicate samples.

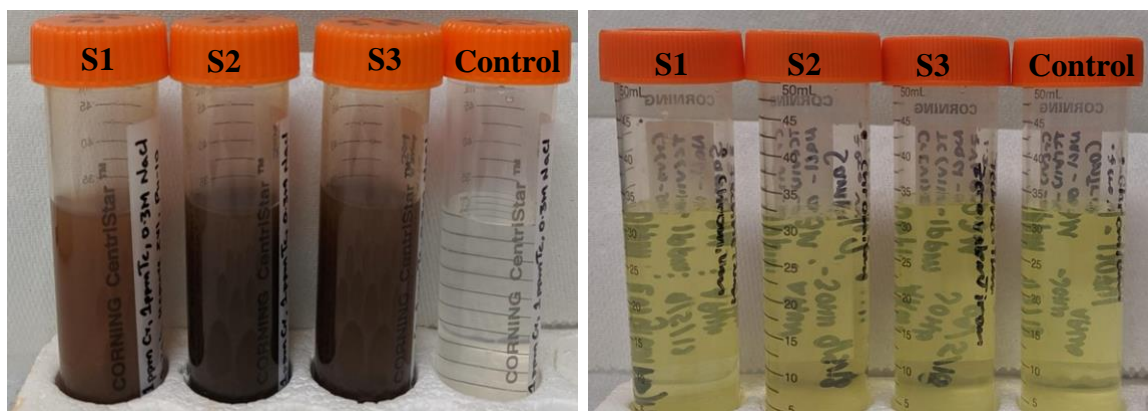


Figure 5. The visual change in the oxidation of iron in triplicate batches amended with high and low concentrations of chromate. 0.3M NaCl, 1mg/L Tc(VII), in basic pH conditions ($\text{pH} = 10.0 \pm 0.1$). Samples aged for 30 days with 1.2 g/L of Hepure ZVI. (Left) Batch containing a “low” initial Cr(VI) concentration of 1mg/L, exhibiting changes in the color of solutions due to iron oxidation and the formation of iron oxides that were further identified by XRD analyses. (Right) Batch containing a high initial Cr(VI) concentration of 50mg/L, with little change to solution color evident of little iron oxidation.

Measurements of common physicochemical parameters

Table 2 lists measurements done on sacrificial samples that were used after 8 days. Lower levels of dissolved oxygen (DO) in a batch containing only 1 mg/L of Cr(VI) versus a batch with 10 mg/L of Cr(VI) support significant differences in iron oxidation depending on Cr(VI) concentration. Lower levels of DO in the solutions signify consumption of oxygen for the formation of Fe(II) and Fe(III) oxides on the surface of the ZVI material. ORP data support the assumption that Tc(VII) might have influenced passivation in the system, as ORP data obtained in batches containing 10 mg/L of Cr(VI) showed an increase in ORP when Tc(VII) was present. Like previous results, a higher pH was seen in samples containing higher concentrations of both contaminants.

Table 2. Oxidation Potential, pH, and Dissolved Oxygen (Aged for 8 Days, 1 mg/L ⁹⁹Tc, 1.2 g/L ZVI, 0.3 M IS NaCl)

Sample Name	Solution Composition	ORP (mV)	pH Final	DO (mg/L)
1 mg/L Cr(VI)	NaCl, Cr(VI)	-	9.66±0.11	0.68±0.13
	NaCl, Cr(VI), Tc(VII)	-	10.14±0.03	0.64±0.13
10 mg/L Cr(VI)	NaCl, Cr(VI)	93.40±18.66	9.42±0.10	1.18±0.72
	NaCl, Cr(VI), Tc(VII)	148.87±45.48	10.30±0.15	2.50±1.69

Solid Analysis via Scanning Electron Microscope

SEM-EDS was used to examine the surface morphology of iron and the elemental composition of dried solids and allowed for qualitative identification of possible iron species present after the reductive separation process. Solids obtained from sacrificial samples prepared for solid analysis after 8 days showed the formation of different iron species. SEM images obtained from sacrificial samples showed different morphological structures which can be identified. Looking at the images obtained, predictions can be made about the species present in the dried solid samples. Surface morphologies found through SEM were used to guide later XRD analysis by having a baseline of what morphologies to look for. Assessing the morphology of iron oxides be used to look for evidence of co-precipitation of reduced Tc with iron. Morphologies that have a likelihood of incorporating Tc have been shown to slow down reoxidation of Tc(IV) to Tc(VII). Effects of performance caused by corrosion inhibition by Tc and Cr can further affect the process by not only inhibiting initial corrosion but also formation of morphologies that are beneficial to prevent reoxidation. Figure 6 and Figure 7 show SEM images of the dried solids. Although singular

iron-oxide species can have different shapes when crystals are formed, some morphologies be more common. For example, goethite can form needle-like, but it is commonly seen in an acicular form. Some common crystal morphologies for iron oxides are described as needle-like, acicular, octahedral, hexagonal, and spiked spheres [15]. The main morphologies found using SEM were spherical and acicular crystals. Acicular formations in both 5 and 10 mg/L Cr(VI) likely indicate the formation of goethite while spherical crystal formations can signify the presence of ferrihydrite [15]. The formation of flake-like structures seen in Figure 7C signifies the possible presence of lepidocrocite [16]. Hexagonal crystals were also seen in less abundance and could signify the presence of hematite which is supported by the brown coloration of the oxidized solids; these hexagonal structures in Figure 8 could also be from the formation of green rust or magnetite [15] which is supported by the magnetic behavior of the iron seen in Figure 9. Batches containing a low concentration of Cr(VI) showed greater coloration caused by iron oxides, while batches with a high Cr(VI) concentration showed very little coloration but showed very high magnetic species, like magnetite.

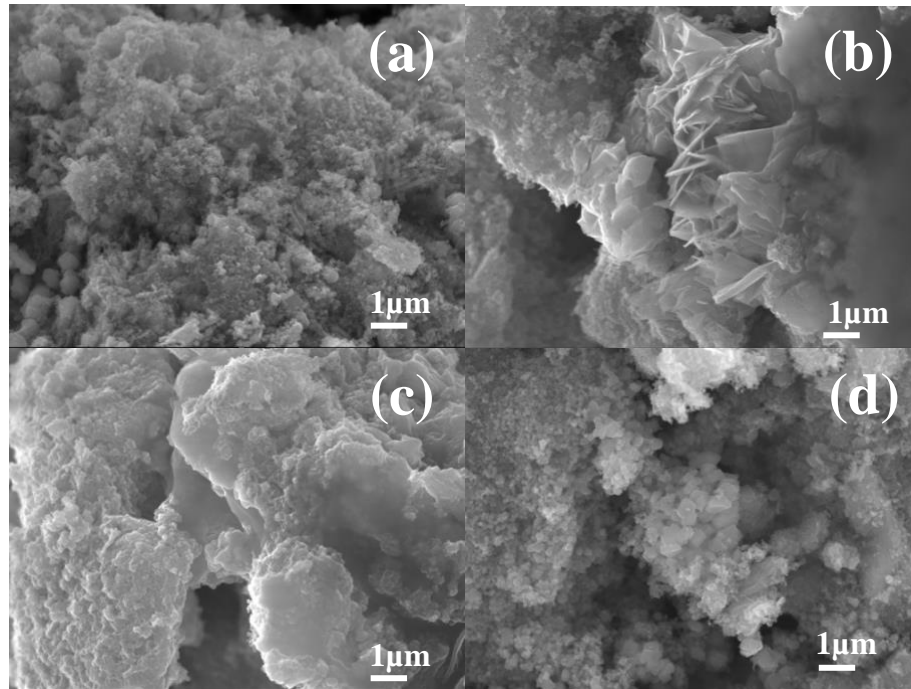


Figure 6. Scanning Electron Microscope (SEM) 8 Day Aged Samples, x10,000 magnified, 20.0 kV. 0.3M NaCl, 1mg/L Tc(VII), 1 mg/L Cr(VI) in basic pH conditions ($\text{pH} = 10.0 \pm 0.1$) with 1.2 g/L of Hepure ZVI. Observed formations will be used to later assess the morphology of the oxidized iron surface. (a) spherical formation, (b) acicular formation, (c) porous formation with surface oxidation, (d) spherical and hexagonal formations.

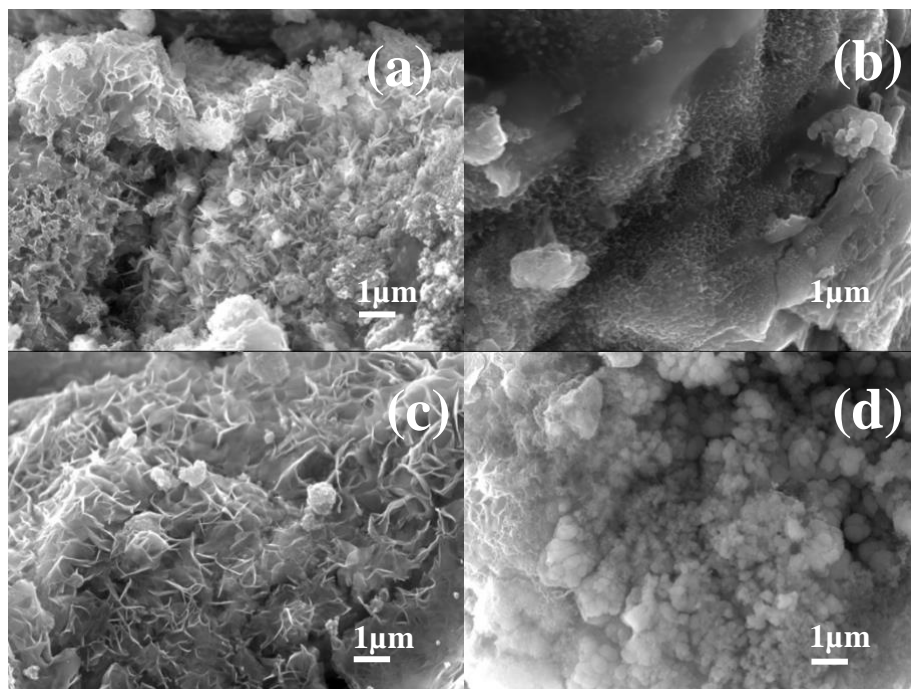


Figure 7. Scanning Electron Microscope (SEM) 8 Day Aged Samples, x10,000 magnified, 20.0 kV. 0.3M NaCl, 1mg/L Tc(VII), 10 mg/L Cr(VI) in basic pH conditions ($\text{pH} = 10.0 \pm 0.1$) with 1.2 g/L of Hepure ZVI. Observed formations will be used to later assess morphology of iron (a) acicular formation, (b) little oxidation with two spherical formations, (c) flake-like formation. (d) spherical formation.

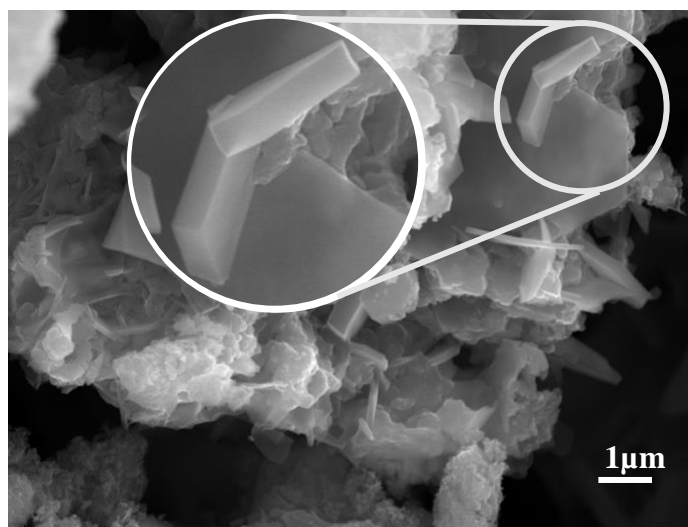


Figure 8. Scanning Electron Microscope (SEM) 8 Day Aged Samples, x10,000 magnified, 20.0 kV. 0.3M NaCl, 10 mg/L Cr(VI) in basic pH conditions ($\text{pH} = 10.0 \pm 0.1$) with 1.2 g/L of Hepure ZVI. Zoomed in is formation of hexagonal iron oxide morphology indicating presence of magnetite [15].

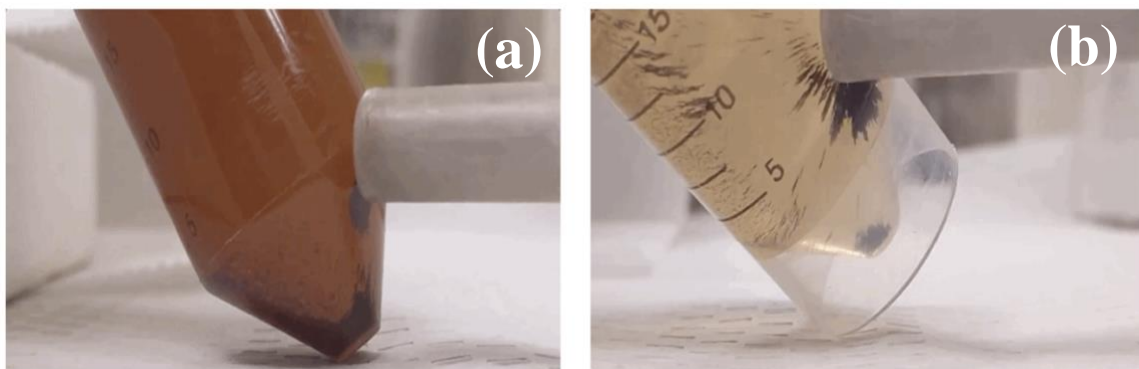


Figure 9. Behavior of iron solids inside batch solutions after 30 days. (a) 1 mg/L Cr(VI) shows brown coloration and some magnetic species. (b) 50 mg/L Cr(VI) shows greater number of magnetic species, with little coloration led by iron oxidation.

Solid Analysis via Energy Dispersive X-ray Spectroscopy (EDS)

Differences in oxidation in dried solids were quantified through an elemental analysis using EDS, as the higher weight percentage of oxygen in the elemental analysis indicates a greater formation of oxidized iron phases. The elemental composition of the dried solids was obtained from the average elemental composition of at least ten different spectra. Figure 10 shows an example of the most representative spectrum from each of the batches that most closely resembled the averages of the ten spectra. When ZVI reduces ^{99}Tc it has been shown to promote removal through adsorption, precipitation, and co-precipitation [9]. Table 3 shows evidence of corrosion inhibition caused by chromium and technetium. Anticorrosive properties of both Cr and Tc are of concern as they can affect oxidation of iron, slowing down the reduction process [11,12]. Solid characterization supported the expected trend of less formation of iron oxides in samples with a $^{99}\text{Tc(VII)}$ and a higher concentration of Cr(VI). EDS analysis informs the inhibition effect that Tc(VII) and Cr(VI) have on iron oxidation. It is likely that high concentrations of Cr(VI) in the off-gas will

affect ZVI oxidation, slowing down treatment; expected off-gas concentration of Cr is high compared to what was tested 1.7mM (~88 mg/L) [3]. Decreased presence of iron oxides like goethite and magnetite, which can incorporate Tc could lead to faster reoxidation of Tc(IV) in off-gas treatment.

Figure 11 and Figure 12 show the full EDS images per each element, where brighter color represents a higher surface concentration of each element. EDS analysis could be used to find evidence of co-precipitated contaminants with iron oxides, which could show more resistance to reoxidation. The weight percentages of precipitated Tc(VII) and Cr(VI) at 1 mg/L in both batches were below the limit of detection of the instrument, hence no precipitated Tc and Cr(VI), or their associations were observed. Quartz was found as an impurity in Hepure ZVI and was present in all solid samples. The approximated mass percentage of oxygen from oxide species was higher in batches containing lower concentrations of Cr(VI). In the future it would be interesting to use high concentrations of Tc(VII) to study co-precipitation of Fe and Tc. The average mass percentage of each element from EDS was used to better estimate different species and morphologies of iron and correlate results with X-Ray Power Diffraction (XRD), this gives more accurate morphological analysis of iron oxides.

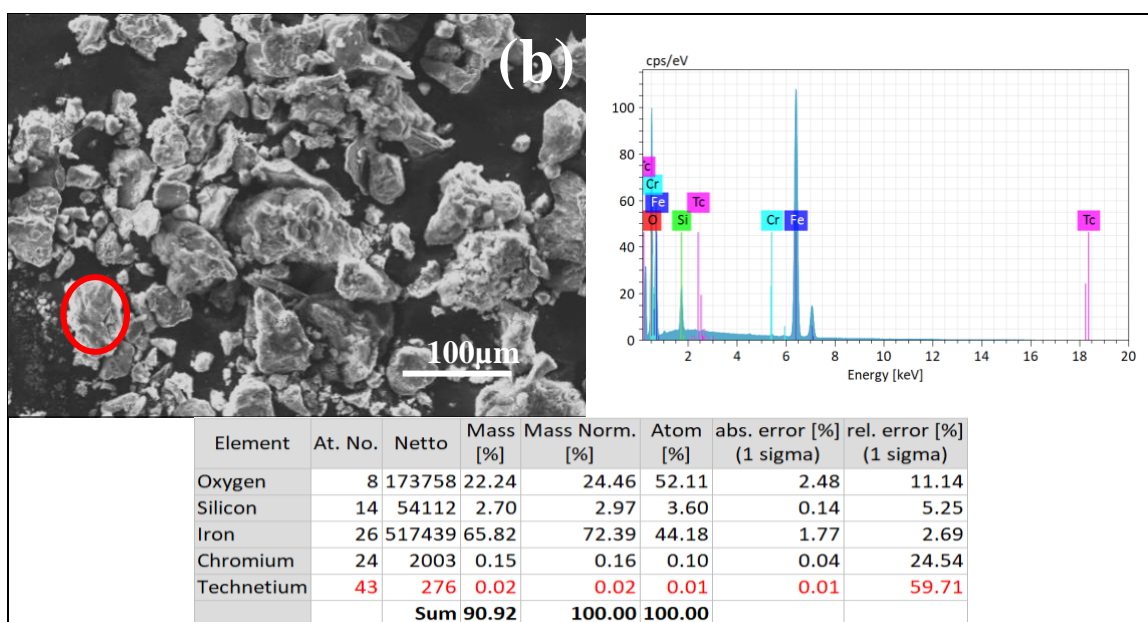
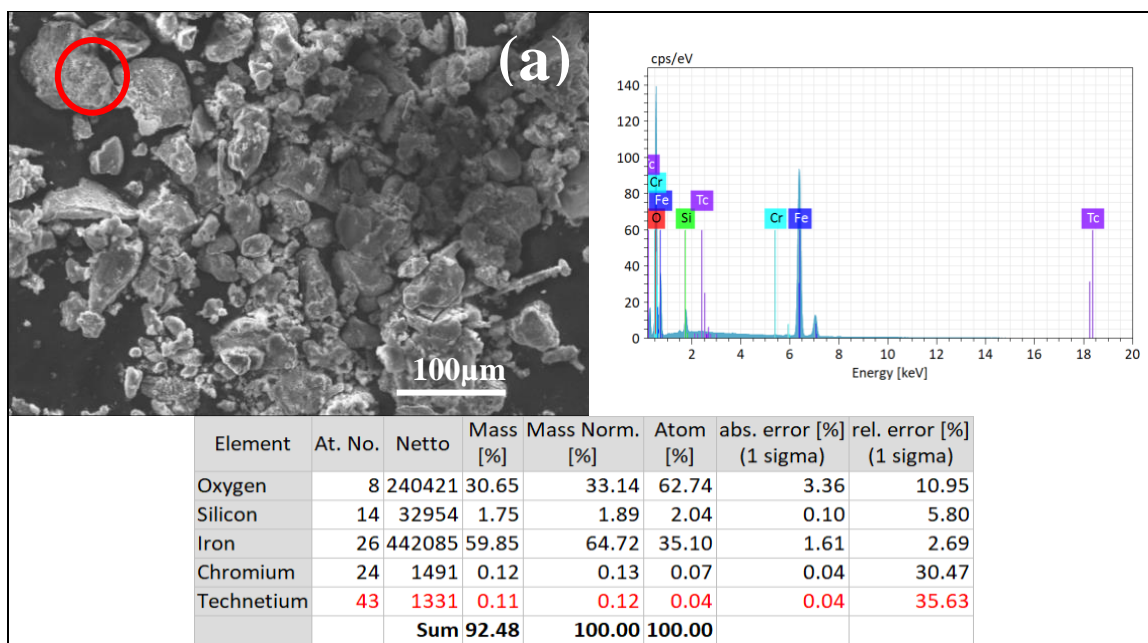


Figure 10. Most representative spectrum from Scanning Electron Microscope (SEM) 8-day aged samples, x250 magnified, 20.0 kV. 0.3M NaCl, 1mg/L Tc(VII), in basic pH conditions ($\text{pH} = 10.0 \pm 0.1$) with 1.2 g/L of Hepure ZVI. (a) 1 mg/L Cr(VI), (b) 10 mg/L Cr(VI). (Left) Shows SEM image with highlighted area of where most representative spectra were collected. (Top right) Shows the collected spectra of SEM, and the elemental matches collected. (Bottom Right) Shows the resulting elemental composition calculated. Note Technetium is highlighted red due to its concentration being below the limits of detection.

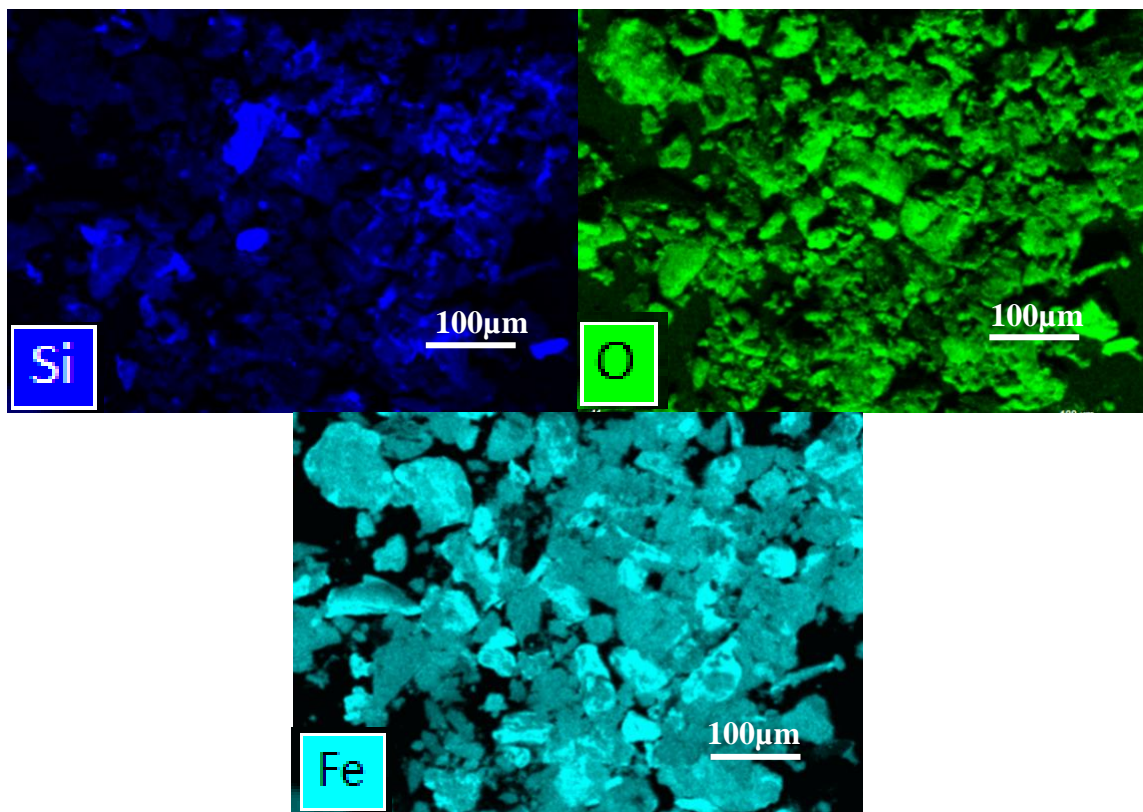


Figure 11. EDS map images from 8-day aged samples, x250 magnified, 20.0 kV. 1 mg/L of Cr(VI) 0.3M NaCl, 1mg/L Tc(VII), in basic pH conditions ($\text{pH} = 10.0 \pm 0.1$) with 1.2 g/L of Hepure ZVI. Brighter areas signify higher weight percentage of each element.

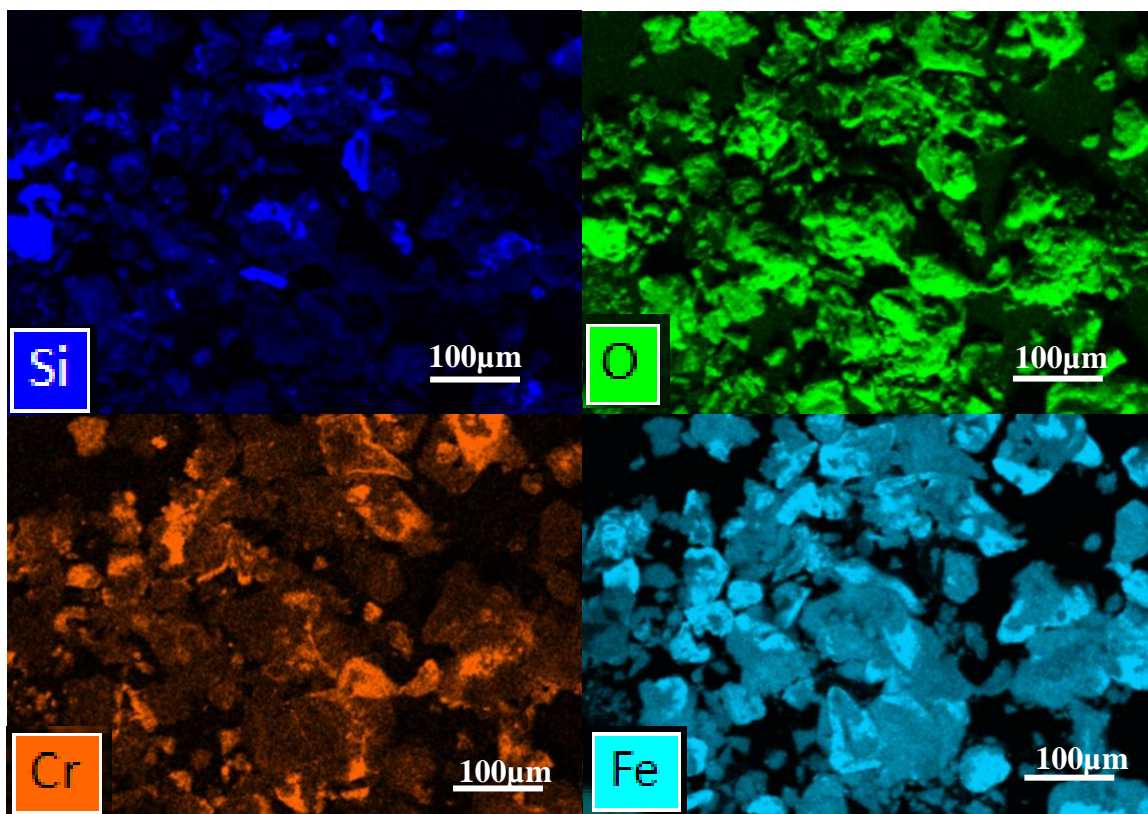


Figure 12. EDS map images from 8-day aged samples, x250 magnified, 20.0 kV. 10 mg/L Cr(VI) 0.3M NaCl, 1mg/L Tc(VII), in basic pH conditions ($\text{pH} = 10.0 \pm 0.1$) with 1.2 g/L of Hepure ZVI. Brighter areas signify higher weight percentage of each element.

Elemental mapping performed with EDS, showed that areas with iron content correlate with higher presence of oxygen, which is consistent with the presence of iron oxides on the iron surface. Brighter chromium regions correlated with lower iron and higher oxygen, suggesting presence of iron-chromium oxides which were later detected by XRD.

Table 3. EDS Elemental Analysis, Average Mass Percentage (Aged for 8 Days, 1 mg/L ⁹⁹Tc, 1.2 g/L ZVI, 0.3 M IS NaCl at variable Cr(VI) content)

Cr(VI) Concentration (mg/L)	Matrix Composition	Average Mass Percentage (%)			
		O2	Fe	Si	Cr
No Cr(VI) (Control)	NaCl,	30.3±9.3	68.1±9.2	1.54±0.69	-
1 mg/L Cr(VI) (Low Concentration)	NaCl,Cr(VI)	30.3±7.3	68.0±7.1	1.95±1.36	-
	NaCl, Cr(VI),Tc(VII)	25.7±10.3	69.9±11.8	4.13±2.63	-
10 mg/L Cr(VI) (High Concentration)	NaCl,Cr(VI)	31.6±7.1	65.3±7.8	0.71±0.53	2.44±1.48
	NaCl, Cr(VI),Tc(VII)	28.3±13.3	71.3±12.4	3.31±1.71	1.28±2.23

Solid Analysis X-Ray Power Diffraction (XRD)

XRD analysis was used to estimate the presence of different iron oxide phases. Figure 13 shows one of the patterns obtained from each of the solids measured and the peaks from the XRD database. The main peak associated with pristine iron decreased according to the amount of iron oxidation seen in each batch. The batches containing the lowest concentration of contaminants showed the greatest decrease in the pristine iron peak, denoting greater oxidation in samples with low contaminant concentration. Based on SEM images, XRD patterns were matched to iron species like magnetite, maghemite and goethite. Other species seen in SEM images were not present in XRD patterns like lepidocrocite, this could be due to low weight percentage of this type of morphology.

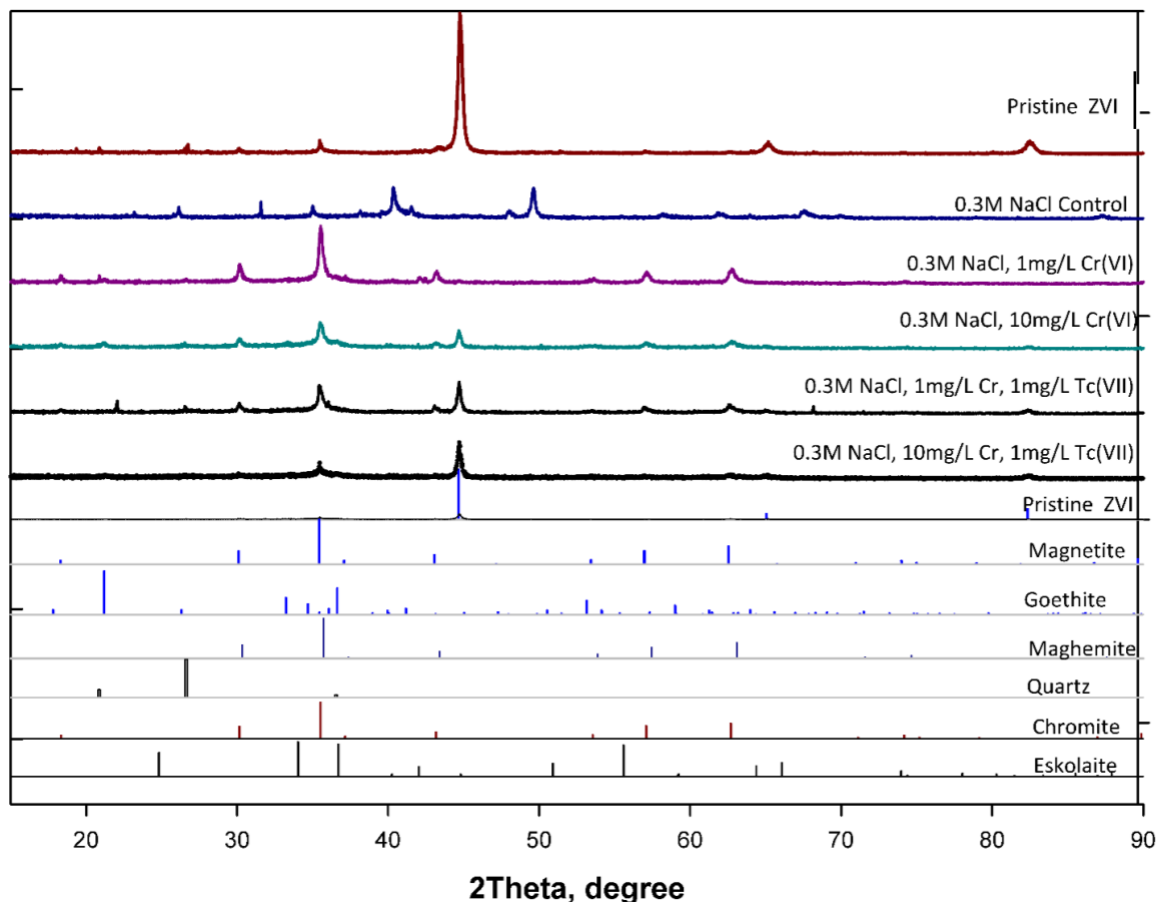


Figure 13. XRD pattern comparison of pristine ZVI (first pattern), and of each of the dried solids from the batch experiments (second to sixth pattern), versus peaks from the Crystallography Open Database XRD database (seventh to eleventh pattern) and International Centre for Diffraction Data's PDF database.

Table 4 shows the different expected iron species and their relative presence in the dried solids. As expected, samples with a higher concentration of contaminants saw a higher percentage of non-oxidized iron. Many iron species seen in SEM images were present but no significant formation of common species like lepidocrocite and hematite were detected in the solid samples through XRD. The presence of Goethite was highest in control batches with no contaminants, indicating a greater degree of oxidation. The addition of ^{99}Tc had significant effects on the oxidation of the iron, batches containing ^{99}Tc had the highest presence of pristine iron, suggesting that ^{99}Tc has a stronger anti-oxidation effect on ZVI

compared to Cr. High presence of species like magnetite and goethite support Tc incorporation in iron oxides [10,17]. Evidence of Tc incorporation in iron oxides could explain the similar reoxidation seen in all batches. When bound to iron minerals immobilized Tc has been seen to be more resistant to oxidation, leading to less Tc mobility [18].

Table 4. XRD estimated percent composition of dried ZVI solids.

[Cr] mg/L	Solution	Fe Iron (%)	Fe ₃ O ₄ Magnetite (%)	Fe ₂ O ₃ Maghemite (%)	FeO ₂ Goethite (%)	SiO ₂ Quartz (%)	FeCr ₂ O ₄ Chromite (%)	Cr ₂ O ₃ Eskolite (%)
0	NaCl	8.6 ±1.8	38.7 ±0.9	16.2 ±6.8	26.1 ±3.7	10.6 ±0.4	-	-
	NaCl Cr	2.8 ±0.9	52.6 ±3.5	26.3 ±1.9	9.3 ±2.1	9.1 ±1.5	-	-
1	NaCl	21.4 ±0.8	41.6 ±3.3	18.4 ±2.1	7.0 ±1.5	11.7 ±4.8	-	-
	NaCl Cr	11.1 ±2.3	35.4 ±1.8	25.5 ±2.6	11.0 ±0.6	9.7 ±1.7	5.1 ±0.4	2.2 ±0.1
10	NaCl	38.4 ±1.5	25.8 ±6.4	12.4 ±1.8	7.7 ±0.6	7.9 ±3.0	5.4 ±0.1	2.6 ±0.6
	NaCl Cr-Tc							

Conclusion

Zero-valent iron shows promising properties for the treatment of radioactive contaminants like ⁹⁹Tc. This study presents the reductive capability of ZVI for removing ⁹⁹Tc with competitive contaminants in the reductive removal process. Hepure ZVI showed the most promising performance for reductive separation compared to other ZVI materials tested. Quick initial removal of Tc for the 24 h of treatment, could be advantageous for the large-scale removal of Tc. A pseudo-second-order kinetic model showed the best linear fit for

the removal of both Tc(VII) and Cr(VI) by Hepure zero-valent iron with higher R^2 values compared to a first-order model.

The remaining fraction of contaminants after thirty days show the limitations of reductive separation. At the highest contaminant concentrations with molar ratios of Fe:Cr of 22 and Fe:Tc of 2113, more than 70% of the Cr(VI) and 30% of the $^{99}\text{Tc(VII)}$ was successfully removed. Batches containing molar ratio Fe:Cr >43 saw complete removal of Tc(VII) after 24-48 hours. Molar ratios could be used to scale up treatment, making it's easier to estimate how much iron is needed versus concentration of Tc and Cr.

Although contaminant reoxidation is of concern, reoxidation of ^{99}Tc did not exceed past 30% for all batches with initial Cr(VI) ≥ 25 mg/L. Future research focusing on the creation of a metallic waste form will determine the limit of how much reoxidation can occur in the manufacturing process. Incorporation of Tc to iron oxides like magnetite and goethite, morphology suggested by both XRD and SEM-EDS analysis, could slow down reoxidation of Tc(IV) [18,19]. Solid characterization showed low formation of iron oxides in samples amended with $^{99}\text{Tc(VII)}$ and higher concentration of Cr(VI) Cr(VI) in the levels expected in the off-gas will affect ZVI oxidation, slowing down treatment. Decreased presence of iron oxides is of concern since it could lead to less incorporation of Tc(VII) or a faster reoxidation. Although Cr(VI) concentration did not affect reoxidation of Tc(VII) in the experiments conducted, changes in iron oxides might have a role in large-scale treatment like the one for the off-gas condensate.

Regarding the treatment of Hanford's off-gas condensate, an alternative treatment as reductive removal poses many advantages compared to re-cycling collected off-gas back into the waste stream. Using high iron loading relative to the concentration of reducible

contaminants could pose for a compelling approach to remove Tc(VII) quickly, reducing costs of the vitrification process. Future research should focus on the production of a metallic waste form after Tc is removed that is viable for long-term storage.

References

1. Gephart, Roy E. "A short history of waste management at the Hanford Site." *Physics and Chemistry of the Earth, Parts A/B/C* 35, no. 6-8 (2010): 298-306.
2. Papagiannopoulou, D. "Technetium-99m radiochemistry for pharmaceutical applications." *Journal of Labelled Compounds and Radiopharmaceuticals*, 60(11), 502-520, (2017).
3. Taylor-Pashow, K. M., McCabe, D. J., & Nash, C. A. "Tc removal from the waste treatment and immobilization plant low-activity waste vitrification off-gas recycle." *Separation Science and Technology*, 53(12), 1925-1934. (2018)
4. Till, John E. "Source terms for technetium-99 from nuclear fuel cycle facilities." In *Technetium in the Environment*, pp. 1-20. Springer, Dordrecht, 1986.
5. Serne, R. Jeffrey, Jarrod V. Crum, Brian J. Riley, and Tatiana G. Levitskaia. *Options for the Separation and Immobilization of Technetium*. No. PNNL-25834; EMSP-RPT-029Rev0. Pacific Northwest National Lab.(PNNL), Richland, WA (United States), 2016.
6. Pegg, Ian L. "Behavior of technetium in nuclear waste vitrification processes." *Journal of radioanalytical and nuclear chemistry* 305, no. 1 (2015): 287-292.
7. Icenhower, Jonathan P., Nikolla Qafoku, Wayne J. Martin, and John M. Zachara. *The geochemistry of technetium: a summary of the behavior of an artificial element in the natural environment*. No. PNNL-18139. Pacific Northwest National Lab.(PNNL), Richland, WA (United States), 2008.
8. Cantrell, K. J., Kaplan, D. I., and Wietsma, T. W., "Zero-valent iron for the in situ remediation of selected metals in groundwater" *Journal of Hazardous Materials*, v. 42, no. 2, p. 201-212. (1995)
9. Boglaienko, Daria, Hilary P. Emerson, Yelena P. Katsenovich, and Tatiana G. Levitskaia. "Comparative analysis of ZVI materials for reductive separation of ⁹⁹Tc (VII) from aqueous waste streams." *Journal of hazardous materials* 380, (2019): 120836.
10. Saslow, S. A., Um, W., Pearce, C. I., Engelhard, M. H., Bowden, M. E., Lukens, W., ... & Kruger, A. A. "Reduction and simultaneous removal of ⁹⁹Tc and Cr by Fe (OH) 2 (s) mineral transformation." *Environmental science & technology*, 51(15), 8635-8642, (2017).

11. Cartledge, G. H. "The pertechnetate ion as an inhibitor of the corrosion of iron and steel." *Corrosion*, 11(8), 23-30, (1955).
12. Cartledge, G. H. "The Mechanism of the Inhibition of Corrosion by the Pertechnetate Ion. II. The Reversibility of the Inhibiting Mechanism." *The Journal of Physical Chemistry*, 60(1), 28-32, (1956).
13. Lide, D. R. (Ed.) *CRC handbook of chemistry and physics* (Vol. 85). CRC press, (2004).
14. Gražulis, Saulius, Adriana Daškevič, Andrius Merkys, Daniel Chateigner, Luca Lutterotti, Miguel Quiros, Nadezhda R. Serebryanaya, Peter Moeck, Robert T. Downs, and Armel Le Bail. "Crystallography Open Database (COD): an open-access collection of crystal structures and platform for world-wide collaboration." *Nucleic acids research* 40, no. D1 (2012): D420-D427.
15. Cornell, Rochelle M., and Udo Schwertmann. *The iron oxides: structure, properties, reactions, occurrences and uses, Chapter 4: Crystal morphology and size*. Page 64. John Wiley & Sons, (2003).
16. Yoon, In-Ho, Kyoung-Woong Kim, Sunbaek Bang, and Min Gyu Kim. "Reduction and adsorption mechanisms of selenate by zero-valent iron and related iron corrosion." *Applied Catalysis B: Environmental* 104, no. 1-2 (2011): 185-192.
17. Um, Wooyong, Hyun-Shik Chang, Jonathan P. Icenhower, Wayne W. Lukens, R. Jeffrey Serne, Nikolla P. Qafoku, Joseph H. Westsik Jr, Edgar C. Buck, and Steven C. Smith. "Immobilization of 99-technetium (VII) by Fe (II)-goethite and limited reoxidation." *Environmental science & technology* 45, no. 11 (2011): 4904-4913.
18. Burke, Ian T., Christopher Boothman, Jonathan R. Lloyd, Francis R. Livens, John M. Charnock, Joyce M. McBeth, Robert JG Mortimer, and Katherine Morris. "Reoxidation behavior of technetium, iron, and sulfur in estuarine sediments." *Environmental science & technology* 40, no. 11 (2006): 3529-3535.
19. Boglajenko, D., Soltis, J.A., Kukkadapu, R.K., Du, Y., Sweet, L.E., Holfeltz, V.E., Hall, G.B., Buck, E.C., Segre, C.U., Emerson, H.P. and Katsenovich, Y., 2020. Spontaneous redox continuum reveals sequestered technetium clusters and retarded mineral transformation of iron. *Communications Chemistry*, 3(1), pp.1-11.